J Mater Sci (2008) 43:4348–4352
DOI 10.1007/s10853-008-2657-3

LETTER

Indentation grid analysis of nanoindentation bulk and in situ properties of ceramic phases

S. Guicciardi · C. Melandri · L. Silvestroni · D. Sciti

Received: 22 February 2008 / Accepted: 14 April 2008 / Published online: 20 April 2008

Composites properties are often derived from the properties of the constituent phases measured in bulk forms. However, in situ properties can be different from those measured in bulk as a consequence of material processing [1–3]. In ceramic composites, for example, spurious phases can form due to the chemical interaction of different powders. The knowledge of in situ properties would allow a better characterization and tailoring of composites performances. Many ceramic composites are particle-reinforced composites so that the evaluation of in situ properties involves measurements in very small volumes. For some mechanical properties, this can be accomplished by nanoindentation tests. By nanoindentation, single microstructural elements can be tested as grains in polycrystals [4, 5] or single phases in composites [3, 6–8]. In this work, a comparison between nanoindentation bulk and in situ properties of some ceramic phases will be presented. Generally, in situ properties are evaluated by imaging the indentation marks, for example using a scanning electron microscope (SEM), to detect which phase was indented. Besides this traditional technique, which can be time consuming especially when indentations are tiny as it happens in hard phases like advanced ceramics, in situ properties will be estimated applying a new type of analysis to nanoindentation data [9–11]. According to this new analysis, the mechanical properties of the constituent phases of a composite can be easily derived from a statistical analysis of nanoindentation results without having to image where indentation marks were placed. Basically, the analysis consists in fitting the experimental data according to a proper number of statistical distributions whose central values correspond to the specific properties of each phase. Constantinides et al. [10] called this analysis indentation grid (IG). In this work, IG will be applied to particle-reinforced ceramic composites, some based on well-known phases, such as $MoSi_2$, Si_3N_4 and TiN, and some based on ultra high temperature ceramics (UHTC), such as HfC and ZrB_2, which are ceramics very difficult to densify in monolithic form [12]. In this way, by IG we also hope to extract properties from relatively dense UHTC phases which cannot be otherwise tested in bulk form. In our investigation, both Young's modulus and hardness will be considered.

The ceramic bulk and particle-reinforced composites to be tested are listed in Table 1 along with some relevant microstructural features. These composites were obtained starting from commercial powders. Detailed information on materials microstructure can be found in Ref. [18] for bulk Si_3N_4, Ref. [19] for HfC + 20 vol% $MoSi_2$, Ref. [20] for ZrB_2 + 15 vol% $MoSi_2$, Ref. [21] for Si_3N_4 + 35 vol% TiN and Ref. [22] for Si_3N_4 + 35 vol% $MoSi_2$. The bulk $MoSi_2$ was specifically produced for this work. The mean grain size of this ceramic material was about 3.0 μm. Specimens from the final pellets were cut, machined and mechanically polished with diamond pastes down to 1 μm. On these polished specimens, nanoindentation tests were performed with a nanoindenter MTS mod. XP (MTS Systems Corporation, Oak Ridge, TN, USA) fitted with a Berkovich indenter. Considering the microstructural scale lengths of the composites to be discussed later on, after some preliminary tests a common peak load of 5 mN was chosen. Care was taken that the tip area function was properly calibrated for the range of penetration depths recorded both in hard and soft phases. This was accomplished by calibrating the area function on a standard fused

S. Guicciardi (✉) · C. Melandri · L. Silvestroni · D. Sciti
Institute of Science and Technology for Ceramics, CNR-ISTEC, Via Granarolo 64, Faenza 48018, Italy
e-mail: stefano.guicciardi@istec.cnr.it

Table 1 Some microstructural features and the Poisson ratio of the produced ceramic materials

Material	Sintering route[a]	Theoretical density (%)	Minor phase mean area diameter (μm)	Major phase Poisson ratio	Minor phase Poisson ratio
Bulk $MoSi_2$	HP	99.0	–	0.15 [13]	–
Bulk Si_3N_4	HP	100	–	0.24 [14]	–
HfC + 20 vol%$MoSi_2$	PS	97.0	2.1	0.18 [15]	0.15 [13]
ZrB_2 + 15 vol%MoSi	SPS	98.1	2.3	0.14 [16]	0.15 [13]
Si_3N_4 + 35 vol%TiN	HP	99.8	3.0	0.24 [14]	0.20 [17]
Si_3N_4 + 35 vol%$MoSi_2$	HP	100	3.1	0.24 [14]	0.15 [13]

[a] HP, hot-pressing; PS, pressureless sintering; SPS, spark plasma sintering

silica specimen. The loading cycle consisted in loading up to the peak load in 15 s and then unloading without any holding time. The contact stiffness was calculated on 90% of the unloading curve. Indentation grids basically consisted of indentations matrices with a space of 5 μm between each indentation. For each material, at least 300 good tests were considered. Based on the analysis of Oliver and Pharr [23], hardness and reduced Young's modulus were obtained by the usual equations from the nanoindenter software (TestWork ver. 4.06a) which automatically corrected the raw load–displacement data for thermal drift and machine compliance. For each material, the empirical distributions of hardness and reduced Young's modulus were created by assigning the probability p_i to the i-datum of the ranked values [24]:

$$p_i = \frac{i}{N} \tag{1}$$

where N was the total number of values for each property, hardness or Young's modulus. The empirical distributions were then fitted with a sum of Gaussian cumulative distribution functions (CDF). Even if in some cases our composites had spurious phases besides the two principal ones, the fitting function CDF was simply taken as the sum of two CDF's whose amplitudes, f_i, were chosen to match the nominal volumetric fractions of the main constituent phases:

$$CDF = \sum_{i=1}^{2} f_i \frac{1}{\sigma_i\sqrt{2\pi}} \int_{-\infty}^{x} \exp\left(-\frac{(u-\mu_i)^2}{2\sigma_i^2}\right) du \tag{2}$$

where μ_i and σ_i are the mean and the standard deviation of the property, Young's modulus or hardness, relative to the i-phase [25]. In complex microstructures, IG analysis can be forced to calculate both mechanical properties and volumetric fractions [25]. However, this complication was out of the main scope of the present article. In case of bulk $MoSi_2$ and Si_3N_4 only one CDF was considered. The non-linear regression of the fitting function of the empirical distribution was performed with the aid of a commercial mathematical software (MATHEMATICA 6.0, Wolfram Inc., Chicago, IL, USA). After the fitting procedure on the reduced Young's modulus results, the mean values of the fitted Gaussian distributions were converted into the Young's moduli of the single phases using the Poisson ratios shown in Table 1. In two composites, HfC + 20 vol% $MoSi_2$ and ZrB_2 + 15 vol% $MoSi_2$, the properties of the constituent phases were also evaluated by a more traditional scanning electronic microscope (SEM) analysis, i.e. by imaging the indentation marks to discern which phase was indented in order to attribute the relative indentation value.

Table 2 summarizes the Young's modulus and the hardness results calculated by IG and SEM analysis both on composites and bulk materials. For the bulk ceramics, the reported values are in agreement with published nanoindentation data for $MoSi_2$ [26] and Si_3N_4 [27]. We will now briefly discuss the IG and SEM results before coming back to the comparison between bulk and in situ values.

The fundamental assumption of IG reflects the basic idea of testing films on substrates: the measured Young's modulus or hardness are representative of the indented particle if the penetration depth is smaller than 1/10 of the

Table 2 Mean values of Young's modulus and hardness as a function of tested phase and evaluation method

Phase	Young's modulus (GPa)		Hardness (GPa)	
	IG[a]	SEM	IG	SEM
$MoSi_2$ bulk	404 (44)	–	20.7 (2.1)	–
Si_3N_4 bulk	303 (19)	–	22.0 (1.4)	–
HfC	497 (13)	494 (41)	28.7 (2.2)	32.4 (1.9)
$MoSi_2$	422 (12)	488 (39)	17.9 (2.0)	18.9 (3.5)
ZrB_2	569 (25)	575 (56)	29.0 (5.6)	33.4 (4.0)
$MoSi_2$	369 (46)	491 (44)	18.4 (1.3)	21.7 (4.1)
Si_3N_4	315 (18)	–	23.5 (2.4)	–
TiN	374 (19)	–	20.9 (5.5)	–
Si_3N_4	334 (14)	–	25.4 (2.3)	–
$MoSi_2$	376 (23)	–	19.5 (2.2)	–

The standard deviation is given in parantheses

[a] IG, indentation grid; SEM, imaging of the indentation marks

radius of an indented particle [10]. However, experiments and finite element simulations have shown that 1/10 is a safety limit for hardness [28]. For the Young's modulus, which is a long-range property [29], this value could be much smaller [30]. Among our materials, composite HfC + 20 vol% $MoSi_2$ had the reinforcement phase with the smallest radius, see Table 1. On this composite, the maximum contact depth recorded in our tests was about 100 nm, i.e. smaller than 1/10 of the radius of the reinforcement, so that the basic assumption of IG was in principle fulfilled justifying the choice of 5 mN as peak load. While this guarantees that the in situ hardness of a phase was not affected by the neighbouring phase, the same cannot be said for the in situ Young's modulus. In the following, however, it will be shown that also this property was unaffected by the proximity of a phase with a different stiffness. Two examples of fitted CDF's are plotted in Fig. 1. The use of CDF instead of frequency histograms avoids the problem of fixing the histogram intervals which can affect the fitting results [25]. As can be seen from Table 2, the in situ IG properties of $MoSi_2$ and Si_3N_4 changed to a more or less extent when passing from one composite to another one. Due to the different histories of the materials, some differences among the various composites had to be expected in force of the different sintering routes, the different spurious phases formed due to the combination of different powders and the different final densities (Table 1). However, also the neighbouring phases could have affected the $MoSi_2$ and Si_3N_4 results. To see if this was the case, in Fig. 2 the IG Young's modulus and hardness of the $MoSi_2$ phase are plotted as a function of the same IG property of the hosting matrix. If the neighbouring matrix had affected the measured value of the indented particle, the hardness and in particular the Young's modulus of the indented particle would have shown a strong correlation with the same property of the neighbouring matrix. As can be seen, instead, there is no apparent correlation between any of the property of the secondary $MoSi_2$ phase and the corresponding property of the matrix phase. In our case, therefore, it can be concluded that the indentation scale length was small enough compared to the microstructural scale length to avoid the influence of the neighbouring matrix on the measured in situ IG properties of the indented phase. The differences observed in $MoSi_2$ and Si_3N_4 phases across the various composites should therefore be attributed to a different microstructure, texture or chemical composition, of these phases. In the HfC, ZrB_2 and $MoSi_2$ phases, the in situ properties were also evaluated by the traditional SEM analysis. As can be seen in Table 2, the agreement between the IG and the SEM analysis results was generally good even if the SEM values were always higher than the IG values. The largest difference, about 33%, was observed for the Young's modulus of the $MoSi_2$ phase in the ZrB_2 + 15 vol% $MoSi_2$

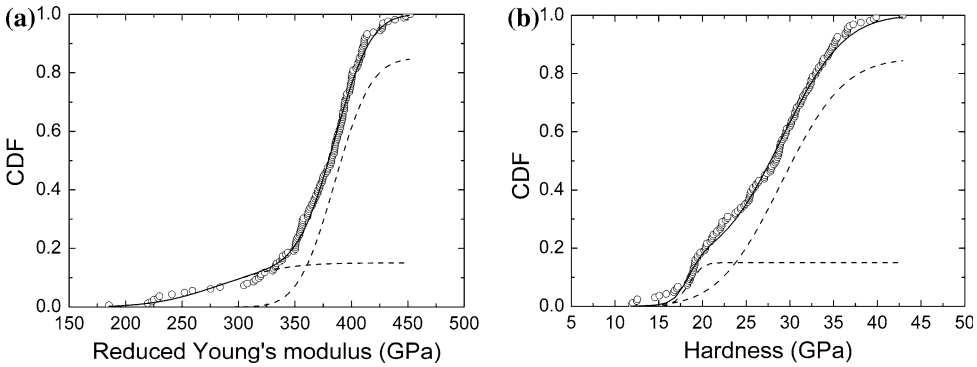

Fig. 1 Empirical distribution (points) and fitted function (solid line) for the ZrB_2 + 15 vol% $MoSi_2$ composite: (**a**) Young's modulus and (**b**) hardness. The individual fitted distributions are shown as dashed lines

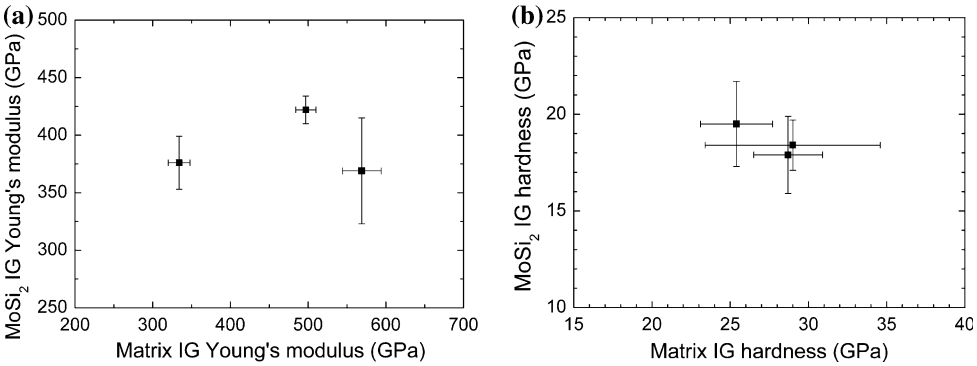

Fig. 2 Plot of the experimental in situ indentation grid (IG) properties of the $MoSi_2$ phase as a function of the same in situ IG property of the matrix: (**a**) Young's modulus and (**b**) hardness. Points and bars represent mean value ± 1 standard deviation

composite. All the other differences between the IG and the SEM values were less than 20%. When a same phase was considered, the SEM results were apparently less influenced than the IG results by the composite under consideration, see in particular the almost identical value of Young's modulus evaluated for the $MoSi_2$ phase in the HfC + 20 vol% $MoSi_2$ and ZrB_2 + 15 vol% $MoSi_2$ composites (Table 2). The higher, and more constant, SEM values can be a natural consequence of the fact that in the IG analysis no filter is applied to the experimental values while in the SEM analysis not well-placed indentations, i.e. those close to pores or phase boundaries, were disregarded. Moreover, by IG analysis spurious phases may have been intercepted which were instead ignored, when indented, in the SEM analysis. Some published bulk values for HfC, ZrB_2 and TiN phases are the following: 461 GPa [15], 500 GPa [31] and 429 GPa [17] for Young's modulus, respectively, and 26.0 GPa [31], 25.3–28.0 GPa [31] and 18.9–21.1 GPa [32], in the same order for hardness. As can be seen, these bulk values are close both to the in situ IG and SEM values also considering that the bulk values were evaluated with methods other than nanoindentation. IG can be therefore considered an efficient and reliable method to evaluate single phase in situ properties in ceramic composites.

Table 2 clearly shows that bulk and in situ properties were different. The differences between bulk and in situ properties did not show a unique pattern: the bulk values were in fact close, higher or even lower than the in situ values. The Young's modulus of bulk $MoSi_2$ was in the range spanned by the in situ IG values, but significantly lower than the in situ SEM values. The hardness of bulk $MoSi_2$ was instead slightly higher than the in situ IG hardness, but in very good agreement with the in situ SEM hardness. In the case of Si_3N_4, both the bulk Young's modulus and hardness were slightly lower than the in situ values. In the worst cases, the largest differences between the bulk and in situ values were about 22 and 16% for the Young's modulus and hardness, respectively. Both these differences were observed in the HfC + 20 vol% $MoSi_2$ composite. Similar discrepancies between bulk and in situ values have been reported for metal–ceramic composites [2] and polymeric composites [3]. The in situ IG results were generally closer to the bulk values than the in situ SEM results. However, this remark does not imply that IG analysis can be intrinsically considered better than SEM analysis in the evaluation of the in situ properties of a phase. More work is necessary in order to ascertain this. At the simple level the IG analysis was carried out for this work, it cannot be ruled out the possibility that IG analysis could have included results which were not related to the two main phases of our composites, as for example results coming from spurious phases, but which could have influenced the final results.

Concluding, bulk $MoSi_2$ and Si_3N_4 materials were tested and compared to the same in situ phases in some particle-reinforced ceramic composites. As expected, the bulk properties were different from the in situ properties in most cases even if the differences were generally not very large. Indentation grid (IG) was used to evaluate the in situ properties of the ceramic phases. It was shown that IG can be considered a valuable tool in order to efficiently extract properties from composites if the indentation length is appropriately scaled to the microstructural dimension. In the tested particulate ceramic composites, it was in fact shown that both hardness and Young's modulus of the secondary phases were not influenced by the neighbouring matrix. Some discrepancies were observed between the results obtained by IG analysis and those obtained by the more traditional SEM analysis.

References

1. Bei H, George EP, Pharr GM (2004) Scr Mater 51:875. doi:10.1016/j.scriptamat.2004.07.001
2. Scholz T, May M, Swain MV, Schneider GA, Claussen N (2003) Z Metallkd 94:819
3. Gregory JR, Spearing SM (2005) Compos Sci Technol 65:595. doi:10.1016/j.compscitech.2004.09.001
4. Ohmura T, Minor AM, Stach EA, Morris JW (2004) J Mater Res 19:3626. doi:10.1557/JMR.2004.0474
5. Viswanathan GB, Lee E, Maher DM, Banerjee S, Fraser HL (2005) Acta Mater 53:5101. doi:10.1016/j.actamat.2005.07.030
6. Campo M, Urena A, Rams J (2005) Scr Mater 52:977. doi:10.1016/j.scriptamat.2005.01.036
7. Wang HF, Nelson JC, Gerberich WW, Deve HE (1994) Acta Metall Mater 42:695. doi:10.1016/0956-7151(94)90267-4
8. Marx DT, Riester L (1999) Carbon 37:1679. doi:10.1016/S0008-6223(98)00239-5
9. Constantinides G, Ulm F, Van Vliet K (2003) Mater Struc 36:191
10. Constantinides G, Chandran KSR, Ulm FJ, Van Vliet KJ (2006) Mater Sci Eng A Struct Mater 430:189
11. Constantinides G, Ulm FJ (2007) J Mech Phys Solids 55:64. doi:10.1016/j.jmps.2006.06.003
12. Opeka MM, Talmy IG, Wuchina EJ, Zaykoski JA, Causey SJ (1999) J Eur Ceram Soc 19:2405. doi:10.1016/S0955-2219(99)00129-6
13. Nakamura M, Matsumoto S, Hirano T (1990) J Mater Sci 25:3309. doi:10.1007/BF00587691
14. Shackelford JF, Alexander W (2001) CRC materials science and engineering handbook. CRC Press, Boca Raton, FL, London
15. Kral C, Lengauer W, Rafaja D, Ettmayer P (1998) J Alloys Compds 265:215. doi:10.1016/S0925-8388(97)00297-1
16. Okamoto NL, Kusakari M, Tanaka K, Inui H, Yamaguchi M, Otani S (2003) J Appl Phys 93:88. doi:10.1063/1.1525404
17. Pang W, Every AG, Comins JD, Stoddart PR, Zhang X (1999) J Appl Phys 86:311. doi:10.1063/1.370730
18. Bellosi A, Monteverde F, Babini GN (1996) In: Babini GN, Haviar M, Sajgalik P (eds) Engineering ceramics '96: higher reliability through processing. Kluwer Academic Publishers, Smolenice, Slovakia, p 197

19. Sciti D, Silvestroni L, Bellosi A (2006) J Am Ceram Soc 89:2668. doi:10.1111/j.1551-2916.2006.01109.x
20. Sciti D, Monteverde F, Guicciardi S, Pezzotti G, Bellosi A (2006) Mater Sci Eng A Struct Mater 434:303
21. Mazzocchi M, Bellosi A (2008) J Mater Sci Mater Med. doi:10.1007/s10856-008-3417-2
22. Winterhalter F, Medri V, Ruffini A, Bellosi A (2004) Appl Surf Sci 225:100. doi:10.1016/j.apsusc.2003.09.048
23. Oliver WC, Pharr GM (2004) J Mater Res 19:3. doi:10.1557/jmr.2004.19.1.3
24. Knight K (2000) Mathematical statistics. Chapman & Hall/CRC Press, Boca Raton, London
25. Ulm FJ, Vandamme M, Bobko C, Ortega JA (2007) J Am Ceram Soc 90:2677. doi:10.1111/j.1551-2916.2007.02012.x
26. Newman A, Jewett T, Sampath S, Berndt C, Herman H (1998) J Mater Res 13:2662. doi:10.1557/JMR.1998.0371
27. Gong JH, Miao HZ, Peng ZJ, Qi LH (2003) Mater Sci Eng A Struct Mater 354:140
28. Durst K, Goken M, Vehoff H (2004) J Mater Res 19:85
29. Johnson KL (1985) Contact mechanics. Cambridge University Press, Cambridge
30. Saha R, Nix WD (2002) Acta Mater 50:23. doi:10.1016/S1359-6454(01)00328-7
31. Bansal NP (2005) Handbook of ceramic composites. Kluwer Academic Publishers, Boston
32. Russias J, Cardinal S, Fantozzi G, Bienvenu K, Bienvenu G (2004) Silicates Indus 69:311